Modeling crystal plasticity with dislocation dynamics simulations: The 'microMegas' code

B. Devincre [1], R. Madec [2], G. Monnet [3], S. Queyreau [4], R. Gatti [1], L. Kubin [1]

(1) LEM, CNRS-ONERA, 29 Avenue de la Division Leclerc, 92322 Chatillon, France
(2) CEA, DAM, DIF F-91297 Arpajon, France
(3) EDF - R&D, MMC, Av. des Renardière, 77818 Moret-sur-Loing, France
(4) LLNL, University of California, Livermore, CA 94551, USA

Keywords: Dislocation Dynamics, Crystal plasticity, Multiscale modeling

1 Introduction

Dislocation motion and interactions are the main processes controlling the plasticity of crystalline solids. When a dislocation glides by an elementary atomic step in a crystal, it shears it locally in a direction and by an amplitude that define its Burgers vector b (1; 2). Such a discrete process contrasts with elastic deformation, where the crystal lattice is only smoothly distorted under stress and in a reversible manner. The elastic theory of dislocations, which mostly derives from Volterra analysis of linear defects in an elastic continuum, provides a good description of the energetics of these defects. Nevertheless, important properties of a dislocation are governed by the highly distorted region surrounding its geometric line, the dislocation core, whose dimension is a few interatomic spacings. Hence, plastic deformation is a complex phenomenon that involves the modeling of many physical processes at different times and length scales.

Simulations of dislocation dynamics and interactions carried out at the mesoscopic scale in the last 20 years, with input parameter values taken from atomistic simulations or experimental measurements, have demonstrated the usefulness of this numerical tool. The aim of dislocation dynamics (DD) simulation is to establish, within a multi-scale approach, connections between dislocation properties at the elementary scale and continuous models for the plasticity of bulk materials. In addition, DD simulations allow fair and direct comparison with experiments. At present, these simulations are considered as a key element for the development of micro- and nano-materials. Indeed, in these materials, the discrete nature of plastic strain can hardly be smoothened out into a continuum framework.

This article presents the methodology used in DD simulation for implementing the motion, multiplication and interactions of dislocation lines in response to an applied load. The technical aspects of simulations on bulk materials, as well as for micro- and nano-samples are discussed. All illustrations are taken from the free software programs 'microMegas[1]'. This simulation code inherits some features from an earlier 'edge-screw' simulation, the very first three-dimensional DD code (3–5) published at the beginning of the 1990s. It also incorporates many original improvements taken from other DD simulations (6–15). The review articles (16) and the previous references may be of interest for retracing a brief history of the DD simulation technique over the last 20 years.

[0]Corresponding author: benoit.devincre@onera.fr
[1]see mM home page at : `http://zig.onera.fr/mm_home_page`

Whereas there are some differences between simulation codes, there are basic features that they all have in common. As explained in Section 2, all simulation codes discretize dislocations into a finite set of degrees of freedom attached to line segments. The forces on these discrete lines are estimated from the elastic theory of dislocations (Section 3) and the positions of the dislocation segments are updated according to material-dependent equations of motion (Section 4). Section 5 presents a more difficult part of DD simulations, which consists in implementing "local" rules that account for dislocation core properties. The last two sections are dedicated to initial conditions and boundary value problems (Section 6) and to concluding remarks.

2 Dislocation line and space discretization

As far as elastic properties are concerned, and like in most DD simulations, the *microMegas* code routinely treats perfect dislocations. This is the most convenient solution for large-scale mesoscopic computations. Nevertheless, specific applications sometimes require the implementation of glissile dissociations, which is easily performed (17; 18). It must, however, be noted that the detail of contact reactions between partial dislocations is poorly known at the atomic scale, except for a few simple materials (19).

As usual in DD simulations, curved dislocation lines are discretized into a succession of straight segments. The main specificity of the *microMegas* code consists in positioning the origins and ends of these segments on a discrete simulation lattice. The latter should in principle have a lattice parameter homothetic to that of the investigated material. To allow for further developments, the discrete sites occupied by the segments extremities are actually restricted to those having cubic symmetry. Then, dislocations in almost compact crystals with non-cubic symmetry can be dealt with by approximation. For example, in the case of Zr (20), an orthorhombic approximation of the lattice was used in order to obtain an ideal hcp cell. This solution implies a distortion of the real lattice by 2.7% along the c axis; it has little effect on the numerical results, as the true elastic constants are used in the computations.

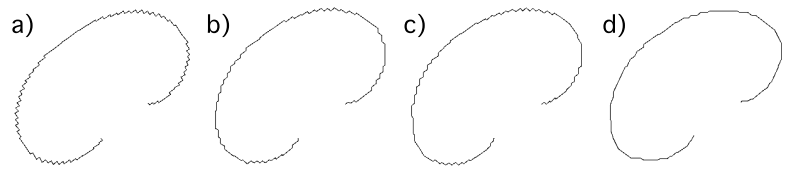

Figure 1: *Four dislocation configurations discretized on a simulation lattice with different line models. The number of segments needed is 121, 100, 91 and 68, respectively, when the number of possible directions per slip system is a) - four; b) six; c) eight (microMegas model) and d) twelve. The critical Frank-Read stresses vary at most by* 3.5%.

As the dislocation configurations are defined on a lattice, the degrees of freedoms are simply defined by the position, length and velocity of the segments. In 3D, the location of a segment is defined from the coordinates of its origin O_i and a vectorial length ℓ_i. This vector defines the direction and length of the segment; it is necessarily parallel to a direction of the underlying lattice. The set of available directions is listed for each slip system as a simulation input. Whereas the original versions of *microMegas* were based on only four directions per slip system (4; 5), the current versions consider a set of eight directions. Such a number is a compromise between opposite requirements. As illustrated by Fig. 1, decreasing the number of segment directions allows describing the curvature of dislocation lines with less segments per unit length (without affecting the simulation results). With more numerous directions the description

is more refined, but the programming of segments motion and reactions with other segments becomes more complex. For many materials, eight segment directions per slip systems represents an optimum value (Fig. 2). Indeed, this solution includes the essential edge and screw directions, but also four additional mixed directions parallel to the slip plane intersections, that is, the junction directions (21). This is fully sufficient to simplify the treatment of the most important dislocation reactions in the most complex crystal symmetries.

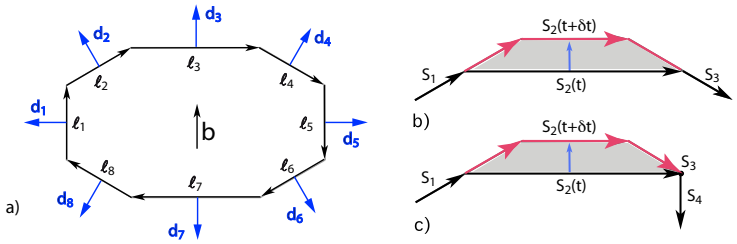

Figure 2: *a) Schematic representation of the elementary vectors used per slip system to discretize dislocation lines in microMegas. The vectors* ℓ_{1-8} *(in black), are used for the definition of the segments directions and the vectors* $\mathbf{d_{1-8}}$ *(in blue) for the corresponding displacement directions. b) and c) Geometrical procedures for the displacement of a segment and its length variation. b) The trapezoidal area swept by segment* S_2 *during a time step* δt *(in grey) produces and increment of plastic shear. This procedure accounts for the direction of the two neighboring segments. c) Before the displacement, a local rule for connections imposes the presence of a "pivotal segment"* S_3 *(segment of zero length) between segments* S_2 *and* S_4.

The definition of a, the lattice parameter of the DD simulation is non-trivial as it constitutes a scaling factor for all distances. Depending upon the problem considered, it can be helpful to set a minimum spacing between slip planes (22) or a minimum distance for dislocation-dislocation interactions. Technically, a can take any value in the simulations, even one that is smaller than the atomic lattice parameter. This last option is sometimes used for performing comparisons with atomistic simulations and to evaluate the limit at which the elastic theory of dislocations looses its validity.

A significant advantage of lattice-based DD simulations is that a large amount of calculations and data can be stored in look-up tables, which reduces the number of operations to be performed per time step. For instance, in *microMegas*, the finite number of segment directions allows tabulating parts of the stress field computations (23). Another important example is related to the displacements of segments. Knowing the directions of the two nearest-neighbors of each segment, the length variations of the three segments can be easily calculated for any displacement amplitude. They can be drawn from a look-up table giving elementary displacements for all possible combinations of the three connected segments. Finally, in lattice-based simulations, most calculations are carried out on integers. They are, therefore, exact when the coordinates of the segment extremities are restricted to sub-lattice sites such that they exclude operations on non-rational fractions. This mathematical aspect is particularly advantageous for simulation procedures treating the detection of forest dislocations or the implementation of periodic boundary conditions. Hence, for each material or type of problem, the definition of an optimal simulation sub-lattice and its associated tables of lengths and displacement vectors is a critical part of the simulation setup. Such tabulations are now available in *microMegas* for the most common crystallographic structures (cubic, fcc, bcc, hcp, dc, etc...).

As the lengths and curvatures of the dislocation lines evolve with time, the discretization procedure must be applied at each simulation time-step in order to add or remove

segments along the lines. As illustrated by Fig. 3, this operation mainly consists into introducing or removing pivotal segments of zero length along the dislocation lines. As changing the line discretization is a discontinuous operation, such changes must be conducted on a fixed geometry. This is why discretization operations can be applied only at the beginning of time steps, before the force computations on segments. Such operations are not trivial and should introduce minimal perturbation of the line configurations, otherwise drastic reductions of the time step would be necessary to reach the final configuration.

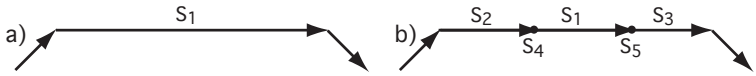

Figure 3: *Discretization of a long segment (S_1) into three shorter segment (S_2,S_1,S_3). In the new configuration, the aligned segments are connected by pivotal segments (S_4, S_5) that constitute additional degrees of freedom distributed along the dislocation line.*

The displacement of a segment induces a variation of the lengths of the two segments to which it is connected (Fig 2). This inter-dependency of the segments lengths implies, for the sake of efficiency, that the length of all dislocation segments be similar and close to the average value $\bar{\ell}_{dis}$ that is specified in the simulation input. Simple discretization procedures are implemented in order to reach this condition. They are applied to all segments, with some specific treatments for particular line configurations. A segment i of length ℓ_i is assigned for discretization and will be discretized into three shorter segments (Fig 3) when one of the following conditions is met:

- $\ell_i > 2\ \bar{\ell}_{dis}$: The maximum length of segments is reached.
- $\ell_i > \bar{\ell}_{dis}$ and the length of one neighboring segment is larger than $\bar{\ell}_{dis}$: Additional degrees of freedom are locally required to better describe the local curvature.
- $\ell_i > 0.5\ \bar{\ell}_{dis}$ and one end of i touches a singularity along the line, like a pinning point, a junction end or a planar defect. A detailed description of the dynamics is locally needed in such cases.

All the operations required to perform these discretizations, as well as several steps involved in the contact reactions of dislocations, imply some reconstruction of the connectivity of the lines. Again, such topological tasks benefit from the finite number of combinations of the segment directions, for which tabulated optimal procedures are available. In short, the main function of these connectivity procedures is to incorporate pivotal segments along the discrete dislocation lines in order to smoothen out the dislocation curvatures. It must be noted that the number of pivotal segments can be up to 30% of the total number of segments in a simulated dislocation microstructure. Given the total number of segments, however, pivotal segments do not bring any additional computing penalty, as they have no length. They do not alter the number of operations involved in the calculations of interaction forces and the collision procedures. Special procedures are nevertheless useful during the computations to eliminate avoidable pivotal segments between two aligned short segments.

3 Force calculation

In a crystal, a stress field $\boldsymbol{\sigma}$ of any origin modifies the total elastic energy. As dislocation motion tends to reduce this energy, dislocations are submitted to a configurational force per unit length, the Peach-Koehler (PK) force. This force is written

$\mathbf{f} = (\boldsymbol{\sigma} \cdot \mathbf{b}) \times \boldsymbol{\xi}$, where $\boldsymbol{\xi}$ is the unit vector associated to the local tangent to a dislocation line of Burgers vector $\mathbf{b}$. Once PK forces are known at reference points along the dislocation lines, the temporal evolution of dislocation configurations can be computed, as shown in the next section. As the PK force only depends on elastic materials properties, its computation is a general and basic feature of all DD simulations.

By reason of symmetry, the integration points (IPs) at which the PK force is calculated are usually set in the middle of segments. Sometimes, the IPs have to be moved to other locations, mostly when they are close to a discontinuity in the curvature of a dislocations line. This typically occurs on segments ending at a junction line or a surface. Then, the IPs are moved to a fixed distance, λ, from the line discontinuity. λ is then a parameter, the distance from a stress field singularity at which the PK force is calculated. The two quantities λ and the simulation lattice spacing a are essential as they allow bypassing the recently developed non-singular continuum elastic model of dislocations (24). For most simulations a value of $\lambda \approx 10b$ is satisfactory.

The total force that is calculated at each IP is decomposed into four contributions deriving from: i) the applied stress field ($\boldsymbol{\sigma}_{app}$) driving dislocation motion, ii) the non local stress field ($\boldsymbol{\sigma}_{int}$) arising from the whole dislocation microstructure except the considered segment, iii) a local line tension accounting for the line curvature close to the IP and, in some cases, iv) an image correction arising from the presence of surfaces and interfaces. It is worth noting that this last contribution is only a small fraction of the total force on most segments (less than a few percent in many problems). It is, however, critical, as it controls some microstructural and confinement effects.

The contribution of $\boldsymbol{\sigma}_{app}$ can be treated in different manners. In simple cases, $\boldsymbol{\sigma}_{app}$ is assumed to be spatially uniform in the simulated volume. Its evolution in time is then determined by a monitoring process that mimicks real deformation tests, for instance in tension or compression. Non uniform stress fields can also be applied. In such cases, discrete solutions defined at reference locations in the simulated volume are interpolated at the segments IPs. These solutions are drawn from either experiment or coupled continuum simulations. An example of the last case is presented in Section 6.

To estimate the force arising on a segment IP from interactions with other segments, the total interaction stress field $\boldsymbol{\sigma}_{int}$ is determined as the sum of the individual fields from all other segments in the microstructure. In isotropic elasticity, there are efficient analytical expressions for calculating these interaction stresses (2; 23). Attention must be paid to the fact that these expressions are mechanically correct only for closed dislocation loops in infinite media. Hence, the fields of dislocation lines ending at free surfaces in finite simulation volumes have to be corrected (25; 26). The solution for the stress field of a straight segment in anisotropic elasticity can be found in (27; 28), but its complexity limits its use in massive simulations; in terms of computing time, the anisotropic computations are one order of magnitude longer than the isotropic ones.

The computation of Peach-Koehler forces is by far the most CPU-consuming part of DD simulations. No matter how efficient is the expression for the stress field of segments, the total amount of operations required for pair interactions scales as O(N2) for a system of N segments. Hence, the computational load quickly becomes too expensive in large-scale simulations. For this reason, numerical algorithms were developed in the past years in order to accelerate force computations.

The fast multipole algorithm (29–31) provides an efficient mean to account for distant interactions. Whereas sophisticated solutions are appropriate for multi-million segments simulations (15), simpler solutions based on the domain decomposition of long-range interactions (see for instance (32)) constitute a good compromise for most simulations. When periodic boundary conditions are used, the evaluation of long-range fields arising from outside the elementary simulation cell is obtained from this last algorithm by summing the periodic contribution of the replicas. For obvious reasons,

this last contribution is usually neglected above one or two layers of replicas.

The main difficulty in implementing parallel computation in a DD code arises from dislocation patterning. Indeed, the standard regular domain decomposition algorithm is not well suited for dealing with the local occurrence of dislocation-rich regions. Simple alternative solutions are, however, available for computations running in modern multi-core workstations. One of them is implemented in the *microMegas* code; it is based on a partitioning algorithm that distributes most of the computation load between CPUs and updates the positions of segments in all the nodes of the parallel calculation at the end of each time step. This simple strategy is RAM-expensive, but gives for most computations a reasonably good load-balance up to 20 CPUs and with more than 10^4 segments. Large-scale parallel simulations require more complex algorithms involving distributed memory (33). This last approach is presently not implemented in the *microMegas* simulation code, in order to facilitate further development of the *microMegas* code by its users.

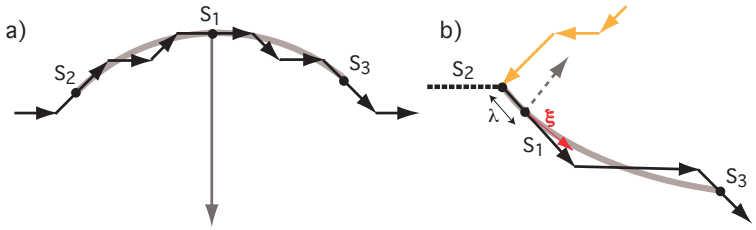

Figure 4: *Regularization procedures for calculating the local line tension of a segment S_1 (schematic). Grey arrows depict the vectorial radius of curvature of the lines at IPs. a) The IPs of S_1 and of two distant segments S_2 and S_3 define an arc of circle. A minimum curvilinear distance is imposed between segments S_2 and S_3. b) Particular case of a segment close to a junction segment (S_2). On the junction side, the arc of circle stops at the extremity of S_2 to account for the presence of a line discontinuity. The unit vector $\boldsymbol{\xi}$ defining the dislocation line tangent at the IP is also plotted. Note that $\boldsymbol{\xi}$ is not necessarily parallel to the segment direction.*

According to the elastic theory, the stress field that a curved dislocation exerts on itself diverges logarithmically at short distances (2; 34). This stress singularity is artificial, and should ideally be regularized by taking into account the physical nature of the core region. This difficult problem was recently investigated by Cai *et al.* (24), who provided a solution that may accommodate some input from atomistic simulations. Nevertheless, most DD simulations are still based on simpler regularization procedures developed in the early days of dislocation theory (34–37). All these procedures lead to an expression for the self-interaction, also called the local line tension, that is proportional to $1/R[\ln(R/a_0) + O(1)]$. R is the local radius of curvature of the dislocation, $a_0 \approx |b|$ is a measure of the width of the core distribution (the core 'radius') and additional first-order geometrical terms are contained in O(1). The uncertainty on the value of a_0 is the main source of error; it leads to significant errors (up to 20%) when R/a_0 approaches unity, as is the case for simulations carried out at the nanometer scale. In the *microMegas* code, four different expressions for the local line tension are pre-defined (34–37). In addition, it is also possible to make use of pre-tabulated line tension values. This last option presents an advantage because it allows implementing the elastically anisotropic line tension in a simple manner with the help of the DisDi code[2] developed by J. Douin (38). For many problems, most of the contribution of anisotropic elasticity is well reproduced in DD simulation by considering only a

[2] see DisDi home page at: `http://pc-web.cemes.fr/Personnel/douin/Disdi-Page`

local anisotropic line tension whose computation is numerically transparent.

There is no well-defined value for the length of the portion of line that has to be regularized at each IP for the force calculations. Practice shows that this length cannot be limited to the nearest-neighboring IPs. The reason is that the segments lengths significantly fluctuate along discretized dislocation lines. Hence, it seems reasonable to set a constant regularization length defined as a fraction of the discretization length (typically $0.2\ \bar{\ell}_{dis}$). Figure 4-a, shows how the local curvature radius entering the expressions for the local line tension is geometrically obtained. From this construction, the local line direction $\boldsymbol{\xi}$ and the dislocation character are determined at each IP. A modified regularization procedure is applied to a few particular IPs, like the ones located close to the triple node of a junction or near a point where the line has cross-slipped. In such cases, the continuous arc of dislocation line is stopped at the point where the line singularity occurs. This procedure is illustrated by Fig. 4-b.

4 Motion and time integration

During a time step in the *microMegas* simulation code, the segments move as a whole in a lattice, in well-defined crystallographic directions and at constant velocity. This topological constraint justifies the definition of a unique IP per segment for evaluating the velocities. This approach with a single IP per segment is not justified for nodal DD simulations, which have to consider non-local schemes for the motion equations (15) or alternative computation strategies based on the principle of virtual work (9; 13; 39).

Once the effective force is known at the IP of segment i, the velocity $\mathbf{v_i}$ is defined with the help of a mobility law. In practice, the line velocity is locally determined by a balance between the elastic PK forces per unit length and a resistive dissipative force, which may arise from the thermally activated motion against the lattice resistance (or Peierls barrier), phonon drag, and other elementary interactions (4; 5; 40; 41). As $\mathbf{v_i}$ is character-dependent in many materials, more than one mobility law is usually defined in a simulation. In *microMegas*, the calculation of the velocity at the IPs is not a function of the segment direction, but rather of the regularized dislocation character as defined in Fig. 4.

In most DD simulations, the specificity of the material considered becomes apparent upon integrating the motion of dislocation segments. Space is missing to present all the currently used velocity laws and only the simplest and most common one is discussed. Defining, τ_i^{tot} as the resolved shear stress related to the total force defined in Section 3 and τ_i^* the effective resolved shear stress that drives the motion of segment i. Then,

$$\begin{aligned} \mathbf{v_i} = 0 \quad \text{if} \quad \tau_i^* \leq 0, \quad \text{with} \quad \tau_i^* = |\tau_i^{tot}| - \tau^f \quad \text{and} \\ \mathbf{v_i} = \text{sign}(\tau_i^{tot}) \frac{\tau_i^* b_i}{B} \quad \text{if} \quad \tau_i^* > 0. \end{aligned} \tag{1}$$

In Eq. 1, τ^f is a dry friction stress parameter accounting for elementary mechanisms such as pinning by impurities and B is a viscous drag coefficient, of which the value is typically 10^{-5}Pa.s in pure metals. This material parameter is temperature-dependent below the Debye temperature and accounts for the dissipative processes associated to dislocation glide (40). In materials with a high lattice resistance, Eq. 1 does not apply and alternative relations accounting for the process of kink-pair nucleation and propagation along the lines are implemented (17; 20; 42; 43).

In quasi-static deformation conditions, the elementary time step is normally taken large enough (a few ns in fcc-like materials) so that inertial effects can be neglected and dislocations glide with a steady state velocity. The explicit Euler forward (EEF) algorithm is the standard method of integration used in DD simulations

$$r(t + \Delta t) = r(t) + v(t)\Delta t \tag{2}$$

When inertial effects have to be included, the Newton equation of motion can always be defined and is complemented by a Verlet algorithm to account for the dislocation effective mass (44–46). The EEF explicit algorithm is preferred in most simulations, whenever its use is justified, as it is computationally inexpensive. The analysis of the stability and accuracy of the EEF integration method provides a simple criterion to fix the simulation time step. A "good" elementary time step, δt, is such that, in average, the mobile segments are predicted to glide over a distance of about $\bar{\ell}_{dis}/100$ per time step. As $\bar{\ell}_{dis}$ depends on the symmetries of the slip geometry and on the scaling of the simulation lattice (2), the optimization of δt is a multi-parameter problem. For instance, a large increase in dislocation density imposes decreasing the simulation lattice and, therefore, the simulation time step. Conversely, in materials with low dislocation mobility, the time steps can be larger, which allows reaching larger plastic strains in an equivalent simulated volume. Besides, it can be noted that the integration of dislocation dynamics is improved when the sequence of segments displacement is performed in a decreasing order of segments velocities. A catalog of velocities is also useful for anticipating intersections with forest segments during a time step (Section 5). Indeed, as the displacements of the segments are treated one after the other, the position of the simulation lattice node where a contact interaction is expected to occur should be preferentially determined in the area swept by the fastest segment.

A recurrent misunderstanding about lattice-based simulations is concerned with the occurrence of artifacts arising from the discrete integration of segments displacements. For instance, it is sometimes erroneously guessed that slowly moving segment should be artificially immobilized when the time step is small. In fact, displacements are performed in the continuum and the positions of the segments are calculated using real coordinates, $r(t)$. The discretized positions, $x(t)$, are defined on the lattice sites nearest to $r(t)$; they are only used in force calculations and in the procedures for detecting segments intersections in order to optimize the computations. For the slow segments, a specific procedure makes use of the difference $r(t) - x(t)$ to reduce the frequency of force calculations. This procedure is equivalent to using a larger simulation time step for slow segments exhibiting real displacements much smaller than the discrete ones.

The interaction between two segments increases rapidly with decreasing distance, which implies increasing velocities in the case of attractive interactions. As dislocation intersections are very frequent in 3D DD simulations, a fraction of these contact interactions should, in principle, lead to a drastic reduction of the simulation time step and of the computing efficiency. For this reason, a maximum glide distance d_{max} and a saturation stress τ_{sat} are defined in *microMegas*. When the effective stress on a segment is larger than τ_{sat}, this segment is supposed to be in an energy basin and its displacement amplitude is reduced to elementary steps of the underlying lattice. Then, the path leading to equilibrium is simply modeled like in a cellular automaton.

A wealth of information is obtained from the motion of segments. We focus here on the calculation of the plastic strain ε^p and the plastic rotation W^p. For a segment i of Burgers vector b_i, the increment of plastic shear per time step is given by

$$\delta\gamma_i^p = \frac{b_i \delta A_i}{V} \tag{3}$$

where δA_i is the area swept during a glide step, and V is the volume of the sheared body. From the increments of plastic shear on any slip system k, one can compute the tensorial increments

$$\delta\varepsilon_{ij}^{p} = \sum_{k=1}^{N} \frac{1}{2}(n_i^k l_j^k + n_j^k l_i^k)\delta\gamma_i^{p^k} \tag{4}$$

$$\delta W_{ij}^{p} = \sum_{k=1}^{N} \frac{1}{2}(n_i^k l_j^k - n_j^k l_i^k)\delta\gamma_i^{p^k} \tag{5}$$

where n_i^k and l_j^k are the components of the unit vectors parallel to the slip plane normal and the Burgers vector, respectively.

5 Dislocation core properties and simulation local rules

In this section, we discuss the treatment of basic dislocation core processes, focusing on the local simulation rules for cross-slip and the modeling of climb, as well as local procedures implemented to account for dislocation contact reactions or interactions between dislocations (annihilation, junction formation) or between dislocations and other crystal defects.

Screw dislocation cross-slip reduces the elastic energy of the crystal; it occurs for screw dipole annihilations, the bypassing of localized obstacles (Fig. 5) and in many other circumstances. This process involves a core transformation and is, therefore, thermally activated in most experimental conditions. Cross-slip events can be modeled using a Monte-Carlo algorithm when the activation energy, which is material-dependent, is known. The rules for cross-slip in fcc materials that were established in (4; 5) were further used in several simulations (13; 30; 47). The probability P for a screw dislocation segment of length ℓ to cross-slip during a time step δt is

$$P = A\frac{\ell}{\ell_0}\frac{\delta t}{\delta t_0} exp\left(\frac{-W}{k_B T}\right), \tag{6}$$

where $\ell_0 \approx 1$ µm and $\delta t_0 \approx 1$ ns are scaling factors, k_B is the Boltzmann constant, T is the absolute temperature and $A \approx 1$ is a parameter adjusted to experiment (5; 48). W is the activation energy of the type of cross-slip process considered, which can be derived from different models. For instance, in relation with the Escaig model (see (49)) and that of Brown (50), the following expressions were proposed for (a) a dislocation immobilized in its glide plane and (b) a moving dislocation (4; 48)

$$\text{(a)}\quad W = V\left(|\tau_{int}^{(g)}| - \tau_{III}\right) \qquad \text{(b)}\quad W = V\left(|\tau_{eff}^{(cs)}| - \tau_{III}\right), \tag{7}$$

where the interaction and effective stresses are respectively resolved in either the glide plane (g) or in the cross-slip plane (cs). V is the activation volume, which is material-dependent and constant as long as the applied stress is not too high, and τ_{III} is the thermally activated critical stress for the onset of stage III in the stress-strain curves of fcc crystals. Values for these two quantities can be drawn from experiment in the most commonly investigated fcc crystals. For other crystal structures, the energetics of cross-slip is poorly understood. In such cases, the expressions used for cross-slip in fcc crystals are applied without justification, or replaced by simple rules (51; 52).

Dislocation climb is a non-conservative mode of dislocation motion involving the absorption of point defects by the lines or their emission. Accordingly, incorporating climb in a DD simulation implies taking into account point defect diffusion in the presence of dislocations. The complexity of such a coupling explains why the vast majority of simulations either only deal with dislocation glide, or treat climb as a

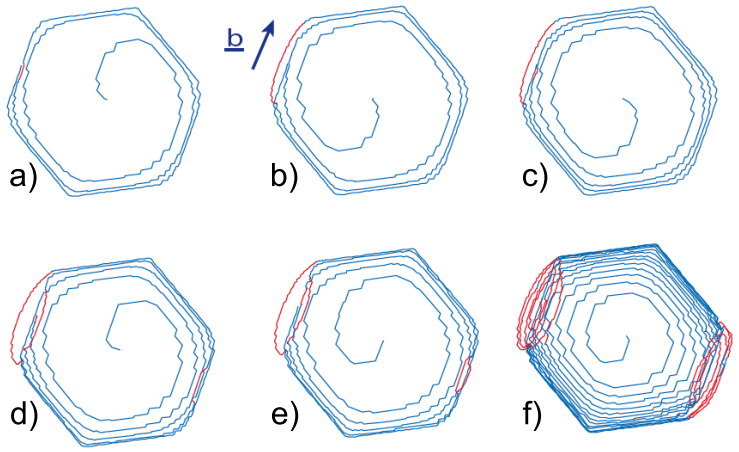

Figure 5: *Relaxation of a screw pile-up produced by a spiral source in a copper grain of diameter 4 μm. The grains boundaries are impenetrable to dislocations. Blue segments: dislocations lying in the glide plane of the source; red segments: cross-slipped segments. The resolved shear stresses are identical in the primary and cross-slip planes.*

kind of conservative glide motion in the climb direction governed by a constant drag coefficient (10; 53). This simplified approach is, however, unable to capture essential features like the temperature dependence of the dislocation climb rate, the high-temperature climb regimes where point-defects are emitted by other dislocations, or the occurrence of dislocation climb without mechanical driving force. This last phenomenon is observed when there is an excess of point defects in the bulk with respect to the equilibrium concentration, for instance under irradiation or after quenching. At present, only a single 3D simulation, which was developed by Mordehai *et al.* (54; 55), is incorporating the coupling of a concentration field of diffusing point defects with dislocation dynamics. It must be noted that in this work, the dislocations only climb but do not glide. Indeed, the simultaneous treatment of these two modes of motion is posing a challenging problem because of the disparity in time scales between climb, which is a quite slow process, and glide that is orders of magnitudes faster.

When two dislocations approach each other at a short distance, their very strong elastic interaction may lead to the formation of particular configurations, which, in turn, affect their dynamics. Two such dislocations typically repel each other locally or adopt a transient attractive configuration that leads to a local annihilation or to the formation of a bound state like a junction, or a crossed state (56–58). As dislocations are linear defects, many short-range interactions and contact reactions necessarily occur during plastic flow. Hence, the ability of a DD simulation to deal precisely and efficiently with the location and by-products of such interactions is a critical issue. The development of *microMegas* (21) was partly motivated by this problem. Indeed, enforcing dislocation motion on a lattice facilitates the prediction of short-range interactions and the modeling of reactions by significantly reducing the number of degrees of freedom.

In *microMegas*, the prediction of short-range interactions encountered by a dislocation segment moving by discrete distances and with discrete lengths variations is quite straightforward. The corresponding algorithm is based on the determination of the intersection between the trapezoidal area swept by the segment (see Fig. 2) and a list of immobile segments or faceted boundaries in its vicinity. Such calculations are extremely fast (even with a large number of segments) if the decomposition of the simu-

lated volume in sub-domains, as defined in the stress field calculations (Section 3), is capitalized with a look-up table of segment neighbors.

At the first potential intersection detected during a time step, the moving segment is stopped upon contact. The method adopted to deal with reactions of non-coplanar segments is illustrated by Fig. 6. First, a special discretization procedure is turned on to inject new degrees of freedom along the dislocation lines. New pivotal segments are introduced on the two lines along the potential reaction direction, that is, along the direction of intersection of the two glide planes. The resulting configuration is considered as a local seed for a dislocation reaction. This initial contact configuration is then let free to evolve under the effect of long-range elastic interactions and the local line tensions. If two portions of lines with Burgers vectors b_i overlap, an effective length of junction is automatically defined at the overlapping portions with a Burgers vector $b_j = \sum_i b_i$ (see Fig. 6 for a description of the two initial configurations that must be considered in the simulations). For simplicity, all junctions are considered as sessile dislocations in *microMegas* whatever the nature of b_j and overlapping segments are immobilized in the initial reaction direction. With uniform loading conditions, this simplifying assumption provides a fairly good description of all the junction contributions to plastic flow (59), including those of the recently discovered multi-junctions[3] (60) (see Fig. 7). The implementation of a more sophisticated description of the junction dynamics including the properties of glissile junctions is a difficult task, but can be realized in lattice based DD simulations (85). This point is regarded as an important future step in the development of the *microMegas* code. Besides, it must be noted that the strength of the present procedure is that the dynamics of junction zipping and unzipping do not require any specific operation. It is simply controlled by the dynamics of the parent dislocation lines.

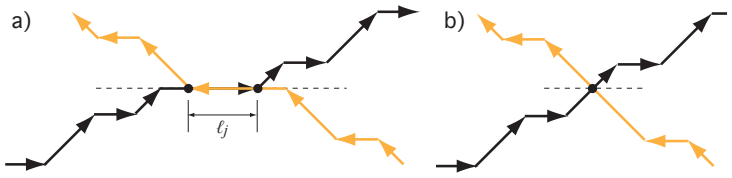

Figure 6: *Junction formation in microMegas (schematic). a) Upon contact between two parallel attractive lines, an incipient junction of length ℓ_j is formed by two portions of line parallel to the direction of intersection of the two glide planes (dashed line). The overlapping lines are discretized and further immobilized, which creates a junction. At the junction extremities, pivotal segments are introduced to let contiguous segments zip or unzip the junction. b) Attractive intersection of two segments initially not parallel to the junction direction. Pivotal segments are introduced at the contact point. In the next simulations steps, a junction can then be zipped just like in a) by the displacement of the contiguous segments.*

Annihilation reactions between two overlapping segments such that $b_j = 0$ are defined in the simulation as a particular type of junction. In such cases, the overlapping sections of dislocation line are removed and additional pivotal segments are introduced along the lines at the extremities of the virtual junction to satisfy the Frank's rule of the conservation of Burgers vector and maintain the continuity of the lines. More detail on this major simulation rule can be found in (61).

The problem of dislocation interactions in a matrix containing a second phase is a complex problem where two different cases have to be considered. If the volume frac-

[3] In *microMegas*, only axial ternary junctions are reproduced, as the modeling of ternary zig-zag configurations implies an exact description of glissile binary junctions

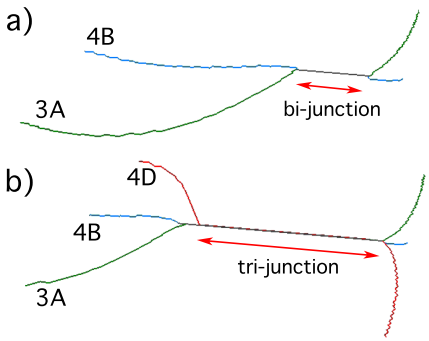

Figure 7: *Binary and ternary axial junction configurations in bcc iron at high temperature under an non-symmetric applied stress. The initial length of the interacting segments is 1 μm. The nature of interacting segments is defined using the notations of Schmid and Boas for slip systems in bcc crystals. a) The first two segments (3A and 4B) form a binary junction with line direction [010]. b) Upon adding the third dislocation (4D), a ternary junction is formed on the initial binary junction direction. Notice that the junction length (i.e., its stability) is larger for the ternary junction.*

tion of precipitates is large and (or) if the interphase has specific properties, there is a boundary value problem to solve, which has to be treated in some detail (Section 6). Alternatively, when considering strengthening by small and distant particles, use can be made of simple local rules (see for instance the work by Mohles *et al.* (62; 63)). Dislocation interactions with small particles (whose coordinates are listed or randomly distributed in the simulated volume) can be represented by a unique variable, a precipitate shearing stress τ_s, whose definition and physical meaning is discussed in the context of *microMegas* simulations (64; 86). τ_s defines a shear resistance related to the mechanical work of the dislocation when it shears a particle with given cross-sectional area in its slip plane. In this framework, the simple case of incoherent precipitates is then reproduced when $\tau_s = \infty$ and the case of coherent precipitates is accounted for with finite values of τ_s (65; 66). Hence, depending on the amplitude of τ_s and the contact length between dislocations and precipitates, a dislocation may or may not shear precipitates When precipitate shearing is impossible, a precipitate can only be by-passed by the so-called Orowan bowing mechanism, that leaves an Orowan dislocation loop around the precipitates. A simulation of this process is shown in Fig. 8. Attention must be paid here to the case of very small obstacles whose bypassing becomes thermally activated and therefore request additional rules in DD simulations.

6 Initial configuration and boundary conditions solutions

Plasticity is well known to be a phenomenon that significantly depends on the thermomechanical history of the sample and on boundary conditions at external or internal surfaces. This sensitivity is even amplified in DD simulations where careful attention has always to be paid to these conditions.
A wide range of initial dislocation microstructures can be used. The simplest configurations contain Frank-Read (FR) sources with various densities, lengths and spatial distributions in the slip systems. Such starting configurations are hardly representative of real dislocation microstructures, which are rather made of three-dimensional networks. A well-known problem of FR source configurations arises from the artificial distribution of permanent pinning points they introduce in the microstructure. In consequence, mechanisms like dislocation starvation or patterning cannot be simulated in a small finite sample with such initial conditions. Artifacts associated with FR sources can be partly eliminated by imposing a large prestrain and cutting out an effective sim-

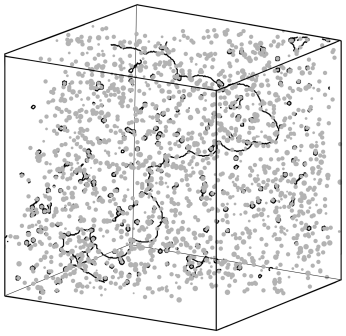

Figure 8: A simulated volume with periodic boundary conditions containing a large density of small spherical precipitates. For clarity, only the precipitates and dislocation lying in a section of thickness 1.5 μm are imaged (65).

ulation volume after relaxation (67). An alternative and very flexible solution, which was utilized in many problems, consists in initiating the simulations with a random distribution of dislocation loops. These loops can be either planar glissile loops or, preferably, prismatic dipolar loops made up of four edge segments with same Burgers vector gliding in two different planes. A relaxation is then performed (with or without applied stress) on this microstructure. A realistic 3D dislocation network is then formed, which is interconnected by junctions and contains no artificial pinning point (68). A interesting discussion on the influence of initial configurations on the modeling of plasticity in sub-micrometric simulated samples can be found in (69).

In many large-scale simulations, the objective is to model plastic flow in a volume representative of bulk conditions. For this purpose, periodic boundary conditions (PBCs) can be applied to reduce the effect of boundaries in the simulated volume (70). PBCs are presently the conditions used by default in *microMegas*. In the past ten years, they have proved to be a very efficient tool for balancing dislocation fluxes at the boundaries of the simulated volume and imposing mechanical equilibrium. However, the use of PBCs in a volume containing tangled lines is a delicate problem (71). In particular, a dislocation loop expanding in a volume with PBCs can undergo strong interactions with its own replica, which may lead to spurious annihilations. The most obvious solution to that problem, which is implemented in *microMegas*, consists of rotating and (or) deforming the simulated volume in such a way as to obtain that the slip planes of dislocations are changed when they re-enter the elementary cell (72). As dislocations must reenter the simulated volume on a crystallographically equivalent glide plane, the number of non-equivalent solutions is finite and specific to the shape of elementary cell. It is worth pointing out that the artifact of PBCs can never be completely eliminated. Hence, the gliding distance of an expanding dislocation before it undergoes strong interactions with its replica must be evaluated in order to define the domain of validity of a simulation in terms of plastic strain. Fortunately, spurious interactions induced by PBCs may be mitigated by the effect of cross-slip on dislocation dynamics.

The elastic interaction between a dislocation and a planar defect, for instance a free surface, is inversely proportional to the distance. Hence the effect of this interaction on dislocations is expected to be small in macroscopic systems and to becomes significant only at very small approach distances of the boundaries. For this reason, it seems natural to assume that image forces matter only for dislocations in volumes of linear dimensions around 1 μm and less. This issue is thus particularly important for the modeling of small confined structures like microelectronic devices or MEMS, which exhibit quite large surface-to-volume ratios. As discussed in some detail by Schwarz (16; 73), it is sufficient in many cases to account for only the force acting on

segments intersecting a surface or an interface. In first approximation, non-contact image forces only modify the velocity at which dislocation are emerging before touching a surface. The effect of a free surface is then to maintain the angle of contact of a dislocation with the surface at a particular value. A physical approximation can be used to determine the latter, which is determined by a compromise between two forces (2; 8), see Fig. 9). The first force arises from the condition of surface mechanical equilibrium and tends to rotate the segment towards the normal to the surface. The second one is quite general, as a dislocation line always tends to rotate towards the screw direction of minimum elastic energy. Taking into account both terms, the local line tension acting on a segment that emerges at a free surface is modified and takes the form

$$\mathbf{f}^{fs} = \frac{\mu b^2}{4\pi(1-\nu)\lambda}[\mathbf{n}_1|(1-\nu\cos^2\beta)\tan\theta|+\mathbf{n}_2|(2\nu\cos\beta\sin\beta)|], \qquad (8)$$

where λ is the distance from the point at which the modified line tension is applied and the point at which the segment intersects the surface. This quantity is a simulation parameter which can be tuned, for instance to reproduce the critical thickness for plastic relaxation in thin epitaxial layers (74; 75).

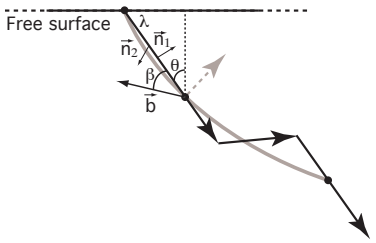

Figure 9: Projection of a segment touching a free surface on its glide plane. Two competing forces act on this segment. One arises from image forces. It depends on the angle θ and tends to rotate the segment towards the normal to the surface. The second one depends on the character via the angle β and tends to rotate it towards the screw direction.

In the last years, more and more complex boundary conditions were used in DD simulations, as illustrated by Fig. 10. The plasticity of multi-phased materials (76; 80), small samples with complex shapes (73) or polycrystalline materials (77) is now mastered. This progress was made possible by the development of numerical couplings of DD simulation codes with FEM codes in order to impose mechanical equilibrium. There are two different approaches four such couplings, namely the *superposition method* (25; 78; 79; 81) and the *discrete-continuous model* (75; 82; 83). For more detail, readers interested in such aspects of DD simulation techniques are referred to a critical review of the two methods (84).

7 Concluding Remarks

In this article, the main features of DD simulations were addressed with emphasis on the *microMegas* code. The progress achieved in the last few years opens the door to more and more complex studies in the plasticity of materials. As illustrated by Fig. 11, one can distinguish two general classes of numerical experiments.

On the one hand, mesoscopic simulations of dislocation dynamics in a representative volume element with periodic boundary conditions, that is, with dimensions comparable to the volume attached to Gauss points in FE methods, can be used to check

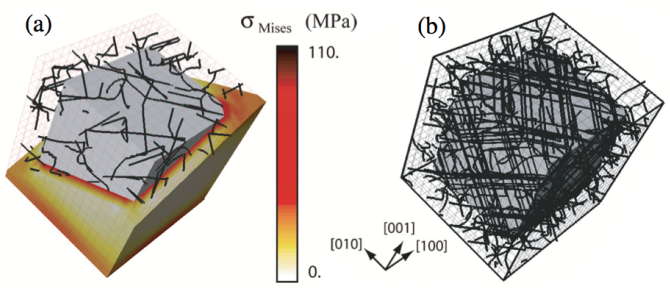

Figure 10: *Example of a MDC simulation applied to a complex boundary value problem (80). In γ/γ' superalloys, the dynamics of dislocations is driven by several mechanical parameters. In a simulated elementary volume, there are misfit and internal stresses at the interface between the cuboid γ' precipitates and the channels of the γ phase. a) The initial dislocation configuration after relaxation. b) After a tensile plastic strain of 0.2 % along the [001] axis.*

and (or) improve physically motivated models for dislocation-based plasticity. In this case, DD simulations function like a numerical coarse-graining method by establishing a connection between discrete and continuous descriptions of plastic flow.

On the other hand, DD simulation is a unique technique for the prediction of plastic properties in micro and nano-objects (including nano-structured materials). Indeed, in sub-micrometric objects the discrete, heterogeneous and discontinuous nature of plastic deformation can hardly be smeared out in a continuum framework. Then, DD simulations can be considered as an upper-scale model for atomistic simulations. The latter are needed to investigate elementary dislocation properties of dislocation, but cannot access large time scales and, therefore, cannot integrate collective properties in dislocation dynamics when they control plastic flow.

Finally, the comparison between experiment and DD simulations certainly has strong potentialities in the expanding domain of local stress and strain fields measurements. Presently, the field evaluations obtained by experimental techniques (TEM, EBSD, x-ray diffraction, DIC, etc ...) cannot be directly related to the mechanical properties of the investigated material. This is because the prediction of plastic properties imply

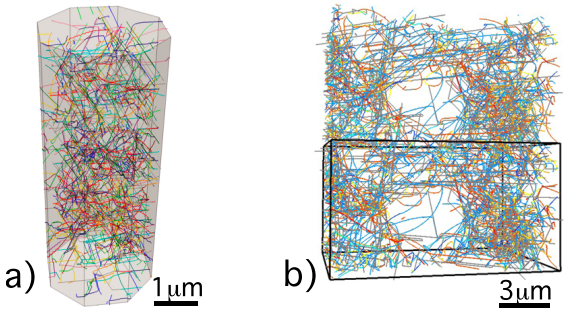

Figure 11: *Two different studies on copper single crystals by DD simulations. a) Size effects: deformation of micropillars. b) Dislocation patterning: cell structure in a* $[001]$ *tensile test. The simulated volume and one replica are shown to illustrate the use of PBCs.*

solving a complex inverse problem. The dynamics of a dislocation is governed by the stress deriving from a Peach-Koehler force on its line. The latter is not the average stress measured in a small surrounding volume element. In addition, experiments usually provide a snapshot of the stress evolution, whereas plastic flow is inherently a dynamic phenomenon. For these reasons, constructing simulated dislocation configurations that reproduce experimental mean-field stresses appears as an attractive, but challenging, approach to a long-standing problem.

References

[1] J. Friedel. *Dislocations*. Pergamon Press, Oxford, 1967.

[2] J. P. Hirth and J. Lothe. *Theory of Dislocations*. Krieger, Malabar (Florida), 1992.

[3] G.R. Canova and L.P. Kubin. In G.A. Maugin, editor, *Continuum models and discrete systems*, volume 2, pages 93–101. Longman Scientific and technical, 1991.

[4] L.P. Kubin, G. Canova, M. Condat, B. Devincre, V. Pontikis, and Y. Bréchet. *Solid State Phenom.*, 23-24:455–472, 1992.

[5] B. Devincre. In H. O. Kirchner, V. Pontikis, and L. P. Kubin, editors, *Computer Simulation in Materials Science*, pages 309–323. Kluwer Academic Publishers, Amsterdam, North-Holland, 1996.

[6] M. Rhee, H.M. Zbib, J.P. Hirth, H. Huang, and T. Diaz de la Rubia. *Model. Simul. Mater. Sci. Eng.*, 6:467–492, 1998.

[7] H.M. Zbib, M. Rhee, and J.P. Hirth. *Int. J. Mech. Sci.*, 40:113–127, 1998.

[8] K.W. Schwarz. *J. Appl. Phys.*, 1999.

[9] N. M. Ghoniem and L. Z. Sun. *Phys. Rev. B*, 60(1):128–140, 1999.

[10] N. M. Ghoniem, S.H. Tong, and L. Z. Sun. *Phys. Rev. B*, 61(2):913–927, 2000.

[11] V. B. Shenoy, R. V. Kukta, and R. Phillips. *Phys. Rev. Lett.*, 84:1491–1494, 2000.

[12] K. W. Schwarz. *Model. Simul. Mater. Sci. Eng.*, 115:609–625, 2003.

[13] D. Weygand, L. H. Friedman, and E. van der Giessen. *Model. Simul. Mater. Sci. Eng.*, 10:437–468, 2002.

[14] V.V. Bulatov and W. Cai. Oxford Series in Materials Modelling. In A.P. Sutton and R.E. Rudd, editors, *Computer Simulations of Dislocations*. Oxford University Press, 2005.

[15] A. Arsenlis, W. Cai, M. Tang, M. Rhee, T. Oppelstrup, G. Hommes, T. G. Pierce, and V. V. Bulatov. *Model. Simul. Mater. Sci. Eng.*, 15(6):553–595, 2007.

[16] K.W. Schwarz. *Multiscale materials modelling: Fundamentals and applications*, chapter Modelling dislocation behaviour at the continuum level. Woodhead Publishing Limited, 2007.

[17] A. Moulin, M. Condat, and L. P. Kubin. *Acta Mater.*, 45:2339–2348, 1997.

[18] A. Vattré, B. Devincre, and A. Roos. *Intermetallics*, 17(12):988–994, 2009.

[19] E. Martínez, J. Marian, A. Arsenlis, M. Victoria, and J. M. Perlado. *J. Mech. Phys. Solids*, 56(3):869–895, 2008.

[20] G. Monnet, B. Devincre, and L.P. Kubin. *Acta Mater.*, 52:4317–4328, 2004.

[21] R. Madec, B. Devincre, and L.P. Kubin. In *Mat. Res. Soc. Symp. Proc. Vol 653*, page Z1.8.1. Materials Research Society, 2001.

[22] J. Lépinoux and L. P. Kubin. *Scripta Metall.*, 21:833–838, 1987.

[23] B. Devincre. *Solid State Communications*, 93:875, 1995.

[24] W. Cai, A. Arsenlis, C.R. Weinberger, and V.V. Bulatov. *J. Mech. Phys. Solids*, 54:561–587, 2006.

[25] E. van der Giessen and A. Needleman. *Model. Simul. Mater. Sci. Eng.*, 3:689–735, 1995.

[26] M. Fivel and G. R. Canova. *Model. Simul. Mater. Sci. Eng.*, 7:753–768, 1999.

[27] M. Rhee, J.S. Stolken, V. V. Bulatov, T. Diaz de la Rubia, H.M. Zbib, and J.P. Hirth. *Mater. Sci. Eng. A*, 309–310:288–293, 2001.

[28] J. Yin, D.M. Barnett, and W. Cai. *Model. Simul. Mater. Sci. Eng.*, 18(4), 2010.

[29] L. Greengard and V. Rokhlin. *J. Comput. Phys.*, 73:325–348, 1987.

[30] M. Verdier, M. Fivel, and I. Groma. *Model. Simul. Mater. Sci. Eng.*, 6:755–770, 1998.

[31] Z. Wang, N. M. Ghoniem, and R. Lesar. *Phys. Rev. B*, 69:174102, 2004.

[32] C. S. Shin, M. C. Fivel, M. Verdier, and S. C. Kwon. *J. Comp. Phys.*, 215(2):417–429, 2006.

[33] W. Cai, V. V. Bulatov, T.G. Pierce, M. Hiratani, M. Rhee, M. Bartelt, and M. Tang. In K. Kitawaga and Y. Shibutani, editors, *Mesoscopic Dynamics of Fracture Process and Materials Strength*, pages 1–11. Kluwer Academic Publishers, 2004.

[34] L.M. Brown. *Phil. Mag.*, 10:441–466, 1964.

[35] A. J. E. Foreman. *Phil. Mag.*, 15:1011–1021, 1967.

[36] S.D. Gavazza and D.M. Barnett. *J. Mech. Phys. Solids*, 24:171–185, 1976.

[37] V. Mohles. *Phil. Mag. A*, 81(4):971–990, 2001.

[38] J. Douin, P. Veyssière, and P. Beauchamp. *Phil. Mag. A*, 54(3):375–393, 1986.

[39] R. V. Kukta and L. B. Freund. *Mat. Res. Soc. Symp. Proc.*, 538:99–105, 1999.

[40] J. Philibert. In P. Groh, L. P. Kubin, and J-L. Martin, editors, *Dislocations et Deformation Plastique*, pages 101–140. Les éditions de Physique, 1979.

[41] W. Cai, V. Bulatov, J. Chang, J. Li, and S. Yip. Dislocation Core Effects on Mobility. In F.R.N. Nabarro and J.P. Hirth, editors, *Dislocations in Solids*, volume 12, chapter 64, pages 1–80. North-Holland, Amsterdam, 2004.

[42] M. Tang, L.P. Kubin, and G. Canova. *Acta Mater.*, 46:3221–3235, 1998.

[43] S. Naamane, G. Monnet, and B. Devincre. *Int. J. Plas.*, 26(1):84–92, 1 2010.

[44] A. Roos. *Fast-moving Dislocations in High Strain-rate Deformation*. PhD thesis, Groningen University, 1999.

[45] E. Bitzek, D. Weygand, and Gumbsch P. In H. Kitagawa and Y. Shibutani, editors, *IUTAM Symposium on Mesoscopic Dynamics of Fracture Process and Materials Strength*, volume 115 of *Solid Mechanics and its Applications*, pages 45–57. Kluwer Academic Publishers, NL-Dordrecht, 2004.

[46] M. A. Shehadeh, H.M. Zbib, and T. Diaz de la Rubia. *Int. J. Plas.*, 21:2369–2390, 2005.

[47] H. M. J.Zbib and T. Diaz de la Rubia. *Int. J. Plas.*, 18:1133–1163, 2002.

[48] C. de Sansal. *Plasticité et effet de taille dans les polycristaux à grains micrométriques*. PhD thesis, Ecole Centrale Paris, 2007.

[49] J. Bonneville and B. Escaig. *Acta Metall.*, 27:1477–1486, 1979.

[50] L.M. Brown. *Phil. Mag. A*, 82(9):1691–1711, 2002.

[51] S. Queyreau. *Etude des mécanismes d'écrouissage sous irradiation de la ferrite par simulations de dynamique des dislocations.* PhD thesis, Universite Pierre et Marie Curie, 2008.

[52] J. Chaussidon, C. Robertson, D. Rodney, and M. Fivel. *Acta Materialia*, 56(19):5466–5476, 2008.

[53] Y. Xiang, L-T. Cheng, D. J. Srolovitz, and E. Weinan. *Acta Mater.*, 51(18):5499–5518, 10 2003.

[54] D. Mordehai, E. Clouet, M. Fivel, and M. Verdier. *Phil. Mag.*, 88(6):899–925, 2008.

[55] D. Mordehai, E. Clouet, M. Fivel, and M. Verdier. *Mater. Sci. Eng.*, 3:012001, 2009.

[56] L. K. Wickham, K. W. Schwarz, and J. S. Stölken. *Phys. Rev. Lett.*, 83:4574–4577, 1999.

[57] R. Madec, B. Devincre, and L.P. Kubin. *Comp. Mater. Sci.*, 23:219–224, 2002.

[58] R. Madec, B. Devincre, and L.P. Kubin. *Phys. Rev. Lett.*, 89:255508(1–4), 2002.

[59] B. Devincre, L.P. Kubin, and T. Hoc. *Scripta mat.*, 54:741–746, 2006.

[60] V.V. Bulatov and col. *Nature*, 440:1174–1178, 2006.

[61] R. Madec. *Des interactions entre dislocations à la plasticité du monocristal cfc; une étude par dynamique des dislocations*. PhD thesis, Université Paris XI Orsay, 2001.

[62] V. Mohles and E. Nembach. *Acta Mater.*, 49(13):2405–2417, 2001.

[63] V. Mohles and B. Fruhstorfer. *Acta Mater.*, 50(10):2503–2516, 2002.

[64] G. Monnet. *Phil. Mag.*, 86(36):5927–5941, 2006.

[65] S. Queyreau and B. Devincre. *Phil. Mag. Lett.*, 89(7):419–430, 2009.

[66] S. Queyreau, G. Monnet, and B. Devincre. *Acta Mater.*, 58(17):5586–5595, 10 2010.

[67] H. Tang, K.W. Schwarz, and H.D. Espinosa. *Phys. Rev. Lett.*, 100:185503, 2008.

[68] B. Devincre, T. Hoc, and L.P. Kubin. *Science*, 320:1745–1748, 2008.

[69] C. Motz, D. Weygand, J. Senger, and P. Gumbsch. *Acta Mater.*, 57(6):1744–1754, 2009.

[70] V. V. Bulatov, M. Rhee, and W. Cai. In *Mat. Res. Soc. Symp. Proc.*, volume 653, page Z1.3.1, 2001.

[71] K. W. Schwarz. *Physical Review B*, 38(4), 08 1988.

[72] R. Madec, B. Devincre, and L.P. Kubin. In H. Kitagawa and Y. Shibutani, editors, *IUTAM Symposium on Mesoscopic Dynamics of Fracture Process and Materials Strength*, volume 115 of *Solid Mechanics and its Applications*, pages 35–44. Kluwer Academic Publishers, NL-Dordrecht, 2004.

[73] X. H. Liu, F. M. Ross, and K. W. Schwarz. *Phys. Rev. Lett.*, 85(19):4088–4091, 2000.

[74] A.E. Matthews, J.W. Blakeslee. *J. Cryst. Growth*, 27:118, 1974.

[75] S. Groh, B. Devincre, L.P. Kubin, A. Roos, F. Feyel, and J.-L. Chaboche. *Phil. Mag. Letters*, 83(5):303–313, 2003.

[76] C.S. Shin, M.C. Fivel, M. Verdier, and K.H. Oh. *Phil. Mag.*, 83(31-34):3691–3704, 2003.

[77] C. de Sansal, B. Devincre, and L.P. Kubin. In *Mechanical Properties of Solids XI*, volume 423 of *Key Eng. Materials*, pages 25–32. Trans Tech Publications, 2010.

[78] D. Weygand, E. Van der Giessen, and A. Needleman. *Mat. Sci. Eng.*, A309-310:420, 2001.

[79] C.S. Shin, M. Fivel, D. Rodney, V. B. Phillips, R. Shenoy, and L. Dupuy. *J. Phys. IV*, 11(5):19–26, 2001.

[80] A. Vattré, B. Devincre, and A. Roos. *Acta Materialia*, 58(6):1938–1951, 2010.

[81] H. Yasin, H.M. Zbib, and M.A. Khaleel. *Mat. Sci. Eng.*, A309-310:294–299, 2001.

[82] C. Lemarchand, B. Devincre, L. P. Kubin, and J. L. Chaboche. In V. Bulatov, T. Diaz de la Rubia, T. Phillips, R. andKaxiras, and N. Ghoniem, editors, *Multiscale Modelling of Materials*, volume 538, pages 63–68. MRS, Warrendale, Pennsylvania, 1999.

[83] C. Lemarchand, B. Devincre, and L.P. Kubin. *J. Mech. Phys. Solids*, 49:1969, 2001.

[84] B. Devincre, A. Roos, and S. Groh. In A. Finel, D. Mazière, and M. Véron, editors, *Thermodynamics, Microstructures and* P*lasticity*, pages 275–284, Dordrecht, 2003. NATO Science Series, Kluwer Academic Publishers.

[85] R. Madec and L.P. Kubin. *Scripta Mater.*, 58(9):767–770, 2008.

[86] G. Monnet, Y. Osetsky, and D. Bacon. *Phil. Mag.*, 90:1001–1018, 2010.